ARTICLE

Check for updates

Dynamic spatio-temporal control of naturally sourced soft photonic crystals

Giulia Guidetti [1], Chris Pirie [2], Giusy Matzeu [1], Giorgio E. Bonacchini [1], Beom Joon Kim[1], Bradley Napier[1] & Fiorenzo G. Omenetto [1,3,4,5 ✉]

The quest for flexible curvilinear displays is driving renewed interest in natural soft photonic systems that rely on the adaptable response of nanostructured living tissues to external stimuli for camouflage and energy management. Understanding and controlling the dynamics of these systems is challenging due to difficulties in sourcing the tissues and constraints in the ability to stimulate them. Here, we present an ex-vivo approach to systematically investigate soft biophotonic crystals and dynamically control their response by using the *Bos taurus* tapetum as a model system. The tapetum's structural color is controlled chemically and electronically and examined by multispectral imaging providing insights on the color change dynamics. The ability to spatio-temporally control the optical response of biophotonic crystals provides insights for the development of soft photonic systems for displays and dynamic light management.

[1] Silklab, Department of Biomedical Engineering, Tufts University, 200 Boston Avenue, Medford, MA 02155, USA. [2] Department of Small Animal Clinical Sciences, College of Veterinary Medicine, Michigan State University, East Lansing, MI 48824, USA. [3] Department of Physics, Tufts University, Medford, MA 02155, USA. [4] Department of Electrical and Computer Engineering, Tufts University, Medford, MA 02155, USA. [5] Laboratory for Living Devices, Tufts University, Medford, MA 02155, USA. ✉email: fiorenzo.omenetto@tufts.edu

Natural photonic crystals often developed in animals and plants as a response to environmental stimuli and are responsible for some of the most brilliant colors found in nature. Different from pigment-based colors, structural colors arise from the interference of visible light with a lattice with a periodic variation of the refractive index at the nanoscale[1–3]. These include systems such as the dynamic guanine-based lattices used by reptiles[4] and marine animals[5,6] for communication and sensing purposes, the collagenous lattices that enable seasonal modulation of visual acuity in ungulates[7], and the lipidic opals in the fronds of brown algae that regulate light harvesting[8]. Some of these structures are adaptable and dynamic, varying their spectral response by changing the physical properties of the photonic lattice for camouflage, enhanced visual acuity, mating, and temperature management, among others. This is achieved, for instance, by pressure changes[4,7], light stimuli[5,6,8], and variations in relative humidity[9] and ionic content within these soft structures[10,11]. The ability to control these systems ex vivo can help understand and mimic the physical principles behind the dynamic coloration of these photonic membranes in vivo. Their full understanding is still lacking due to issues in sourcing (photonic structures are more easily found in tropical environments and protected species[12]), in the limited size of the photonic lattice (often less than a few cm^2), and in constraints in the type of stimuli and interfaces that can be used to tune and evaluate their optical response.

Biomimetic ex vivo control of natural photonic structures has been achieved by various strategies including a variation of pressure[7], and changes in osmolarity[4,11] and the refractive index contrast[13–15]. Fine control of the optical response of organisms with biologically relevant coloration can be obtained also using electrical impulses. Electrical impulses can regulate the spectral response of photonic crystals by inducing chemical changes through oxidation and reduction processes or acid and base exchanges that affect the lattice geometry[16,17]. This latter strategy has been reported for pigment-based systems such as the chromatophores of cephalopods[18] but not yet documented for natural photonic structures.

This work uses the collagen-based *Bos taurus* tapetum as a model system for naturally occurring structural color, investigating ex vivo control of its photonic response and systematically quantifying its response dynamics. The tapetum is first characterized in static conditions; then its reflectance is modulated across the visible range both using pH variations and electrical stimuli interfaced using pH buffers and electrode arrays, respectively (Fig. 1).

Natural photonic structures are commonly located in some of the outermost layers of the hosting organisms due to their biological roles often linked with communication purposes and light-harvesting[19]. Interestingly, crepuscular animals and animals active in low light environments have developed intraocular photonic retroreflectors in their eyes[20] to increase their visual sensitivity as a response to either variable or low light conditions. These systems are known as tapetum[21], which means "shiny tapestry" in Latin; despite being documented, the tapetum's structure, composition, and optical properties are still elusive in most species (Fig. 1a–c)[22].

The tapetum can be found either within or behind the retina. Tapeta are nanostructured soft photonic tissues that usually consist of arrays of individual high refractive index scatterers arranged in a low refractive index soft matrix (Fig. 1a, b). Upon interference with visible light, they work as photonic retroreflectors by selectively reflecting light in the visible range[20,22–24]. The tapetum's biological role is to reflect back to the retina the photons that were initially not absorbed by the photoreceptors thus providing these photons with a second opportunity to be absorbed by the retina; this retroreflection mechanism decreases the threshold for light stimulation, allowing animals to see even in minimal illumination conditions (Fig. 1b)[21,23,25]. Tapeta have been documented for various animals, including mammals[7,23,26–29], reptiles[22], arachnids[30], mollusks[31,32], and fish[33–35]. Interestingly, each species seems to have developed the tapetal structure to reflect the wavelength most relevant for the

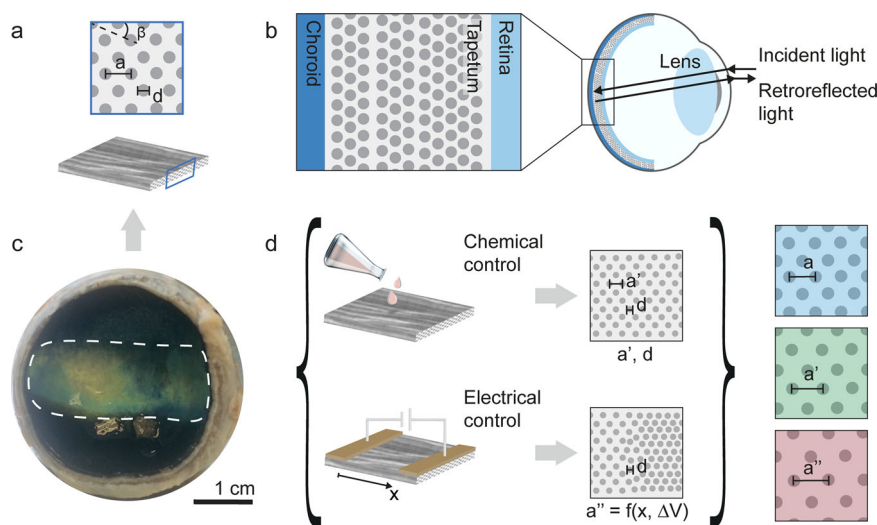**Fig. 1 Spectral control of naturally sourced soft photonic crystals. a** Schematic representation of the bovine tapetum photonic structure in cross-section (top) and perspective view (bottom). The collagen fibrils (diameter d) are arranged in a 2D photonic crystal with lattice constant a and lattice orientation β with respect to the surface of the tapetum. **b** Schematic representation of the multilamellar organization of the collagen photonic crystal forming the tapetum (left) and of the bovine tapetum location within the eye (right). **c** Macroscopic picture of an enucleated bovine eye showing bright green–yellow reflection in the superior fundus region corresponding to the tapetum fibrosum (dashed white line). **d** Schematic representation of the strategies used to control the optical response of the tapetum in the visible range. Chemical changes in the environment surrounding the tapetum are used to induce variations of the optical response that are macroscopically uniform over the tapetum surface area (a'); the application of voltage differences using electrode arrays induces lattice variations that depend on the lattice relative position with respect to the electrodes and on the applied voltage (a'' depends on the position x and applied voltage ΔV) and can reach microscale resolution.

species' living conditions[25,35]. Despite extensive morphological studies of the tapetum, their optical characterization has been documented only for a few species[7,30,32,34], therefore, hindering a comprehensive understanding of the mechanism of vision enhancement.

Typically, bovine tapeta are elongated rectangular membranes restricted to the central part of the superior fundus of the eye (Fig. 1c), on top of an absorbing choroidal layer and underneath the animal's retina (Fig. 1b, Supplementary Figure S1, S2). They generally have a reflective appearance spanning from blue to red with heterogeneities in shape and color given by the variability of naturally occurring tissues. Bovines have a tapetum fibrosum made of collagen fibrils arranged in a 2D photonic structure with hexagonal symmetry (Fig. 1a)[28,36]. The optical response of bovine tapeta thus depends on the collagen fibrils diameter d, the lattice constant a, the orientation of the lattice with respect to the surface of the tapetum β, and on the refractive index of the fibrils and of the matrix (Fig. 1a)[2,3]. In practice, the larger the lattice constant, the more redshifted the light reflected from the tapetum is, assuming the other parameters remain constant (Fig. 1d). Bovine tapeta are straightforward to source[37] and of a size considerable enough (~cm^2) to allow for ex vivo manipulation of the optical response using chemical and electrical strategies both uniformly across the tapetum surface area and in patterns (Fig. 1d).

This work systematically investigates the optical response of soft biophotonic crystals sourced from *Bos taurus* tapetum. The tapetum color is reversibly tuned using chemical and electrical stimuli that can either uniformly affect the entire surface area or only specific regions of the tapetum. The color change dynamics in variable pH environments and electric fields are visualized using multispectral imaging. The ability to spatio-temporally control the optical response of soft biophotonic crystals is useful for the development of tunable soft photonic systems with dynamic spectral response.

Results and discussion

Bovine tapetum static characterization. The static conditions under which the tapetum was studied correspond to the photonic structure being free-standing and immersed in deionized water (pH 6.6). Bovine tapeta from *Bos taurus* have a broadband optical response in the visible range (Fig. 2), with a colorful stripe-like reflective optical appearance (Fig. 2a). The rich color response of the tapetum is studied using bright-field multispectral microscopy, since this technique allows collecting 3D image stacks that contain the spectral fingerprint of every pixel of the image, thus resulting in spectrally-resolved maps of the reflectance of each single-colored region in the tapetum[38,39]. Depending on the imaged region on the tapetum, numerous reflective contributions spanning the entire visible range can be isolated (Fig. 2b, c). The isolation of the individual spectral components and their representation in false-color spatial maps (Fig. 2b, $\lambda_{465\,nm} - \lambda_{750\,nm}$) allows for the visualization of the spatial location of each reflected contribution. These spatial maps show how neighboring spectrally uniform regions display a continuous change in reflectance with a smooth transition from one spectrally uniform region to the next one (Supplementary Fig. S3); this optical response suggests the lack of proper domain boundaries as typical of low-range order structures and as also confirmed by transmission electron microscopy (TEM) images (Fig. 2f, g). Conversely, the recombination of the individual spectral components into a single map (Fig. 2b, combined) provides a straightforward global visualization of the rich spectral response of the tapetum, which would otherwise not be possible by investigation of the RGB image alone (Fig. 2b, RGB). This richness in the optical response indicates the presence of short-range order at length scales

comparable to optical wavelengths. Scanning electron microscopy (SEM) and TEM images confirm that long-range macroscopic uniformity is lacking (Fig. 2d, f and Supplementary Fig. S4), while at the micrometer scale there is higher uniformity in the orientation and lattice parameters (Fig. 2d, f, g and Supplementary Fig. S4)[40], thus accounting for a more narrowband spectral response at this scale and for the uniform color observed within the individual stripes bundles (Supplementary Fig. S3)[41]. Discontinuities in the 2d arrangement of the collagen fibrils[42] are particularly visible between adjacent lamellae (Fig. 2f and Supplementary Figs. S4, S5) and are also accentuated by the buckling of the tissue upon enucleation.

The photonic lattice in the *Bos taurus* tapetum is formed by micrometer-long collagen fibrils as scattering elements, hexagonally arranged in an aqueous, negatively charged, and rich in proteoglycans[43] matrix, with average refractive index $n_{tapetum,\,wet} \sim 1.42$ when hydrated and $n_{tapetum,\,dry} \sim 1.54$ when dry[44] (Supplementary Fig. S6). The collagen fibrils exhibit the typical absorbance peaks given by the amide groups, as demonstrated by Fourier-Transform Infrared Spectroscopy (FTIR): amide I (centered at 1638 cm^{-1}), amide II (1534 cm^{-1}), and amide III (1231 cm^{-1}) (Fig. 2j). Also, the characteristic cross striations caused by the staggered parallel arrangement of each helicoidal tropocollagen unit are visible in TEM images (Fig. 2e)[28,43,45,46]. The striation spacing ($D_{striation} = 64.7 \pm 6.8$ nm, avg ± s.d., $n = 276$) is consistent with previously reported data for bovine eyes[28]. Similarly, the collagen fibrils diameter ($d = 143.30 \pm 15.00$ nm, avg ± s.d., $n = 2286$) and the lattice constant ($a_{lattice} = 171.91 \pm 28.75$ nm, avg ± s.d., $n = 2072$) in the hexagonal lattice are at the scale necessary to generate a photonic response in the visible range (Fig. 2h, i) and consistent with previously reported morphological data[28,46] despite possible lattice distortions caused by the sample preparation for transmission electron microscopy.

Bovine tapetum dynamic characterization. The ability to control and examine the dynamics of naturally occurring soft photonic systems is explored with an ex-vivo approach that allows systematically investigating these constructs and dynamically controlling their response by applying external stimuli. The optical response of the bovine tapetum can be reversibly controlled from the macro to the microscale by using a variety of stimulation strategies including mechanical (Supplementary Fig. S7), chemical (Fig. 3), and electrical (Fig. 4) stimuli.

pH driven dynamic behavior of soft-photonic systems. Ex vivo control of the optical response of the tapetum is obtained by modulating the chemical environment surrounding the photonic structure, which can affect the physical parameters of the photonic lattice (Fig. 3). pH-driven variations in the electrostatic interaction between the scatterers of a photonic system induce compression/expansion of the photonic lattice and thus a variation in the optical response[16]. The aqueous matrix separating the collagen fibrils in the tapetum is rich in proteoglycans which impart a negative charge to the interfibrillar space and thus dictate the electrostatic interaction between adjacent fibrils[43]. Variations in the pH surrounding the tapetum are thus expected to affect the lattice of the tapetum as it follows: acidic environments decrease the electrostatic repulsion given the by negatively charged proteoglycan-rich gel, thus allowing the collagen fibrils to pack more tightly; this implies a reduction of the lattice constant and thus a blue-shift of the reflected light. Conversely, basic environments increase the electrostatic repulsion between the fibrils and induce a less tight packing of the fibrils which results in a red-shift of the light reflected from the tapetum. To test this
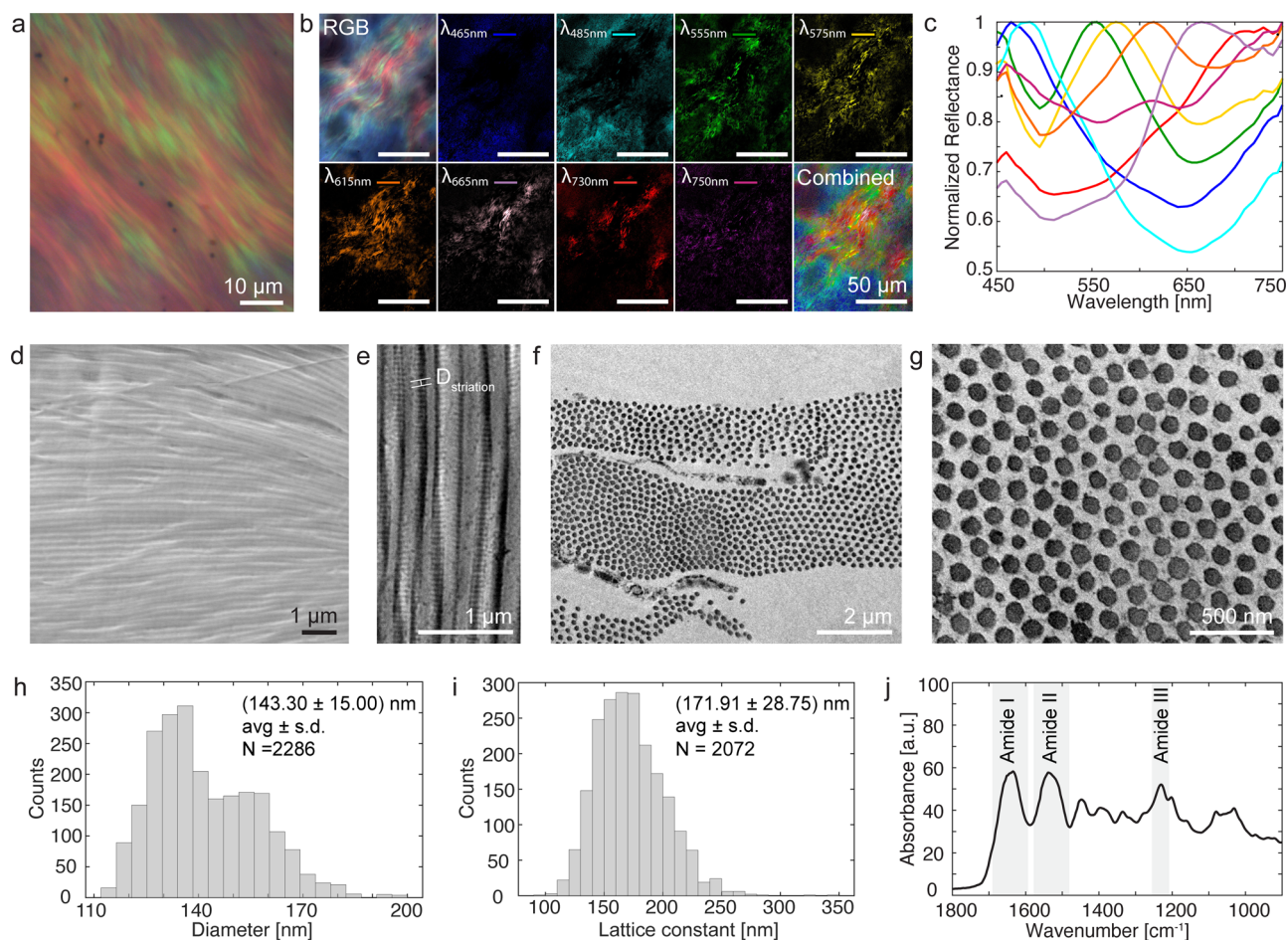
Fig. 2 Static characterization of naturally sourced soft photonic crystals. a Brightfield reflectance micrograph of a region of the tapetum reflecting in the visible range. **b** Multispectral mapping of bovine tapetum: RGB, individual spectral components ($\lambda_{465nm} - \lambda_{750nm}$), and recombined false-color bright field reflection micrographs of the bovine tapetum showing color richness caused by the low-range order of the 2D photonic structure. **c** Corresponding reflectance spectra for each spectral component in the 450–750 nm range. **d** Top-view scanning electron micrograph of the tapetum showing parallel-arranged collagen fibrils. **e** Top-view high-magnification transmission electron micrograph of a bundle of collagen fibrils displaying the typical cross-striations with average spacing $D_{striation}$. **f** Cross-sectional view of a low-magnification transmission electron micrograph of the multilamellar structure of the tapetum. **g** Cross-sectional view of a high-magnification transmission electron micrograph of the 2D hexagonal photonic lattice. **h** Size distribution of the collagen fibrils' diameter. **i** Size distribution of the 2D lattice constant. **j** Representative FTIR absorbance spectrum of dry tapetum showing the typical amide I, amide II, and amide III collagen bands.

hypothesis, the bovine tapetum optical response was monitored as a function of gradual pH changes (Fig. 3a–e and Supplementary Fig. S8) and pH swings (Fig. 3f–j). Due to the striated appearance of the tapetum, to determine the representative behavior of this biological tissue, the tapetum was imaged at low magnification in brightfield reflection and the spectral signal was collected from a large area, (33–45 μm conjugated diameter of the fiber spot), thus contributing to the relative broadness of the reflection spectra (Fig. 3e, j and Supplementary Fig. S8).

The gradient in the pH of the chemical environment surrounding the tapetum was established by using a citrate-phosphate buffer adjusted with the addition of NaOH and HCl, to obtain a basic and an acidic environment, respectively (Fig. 3a), starting from an almost neutral environment (Supplementary Fig. S8). When switching from acidic to basic conditions, the intensity of the light reflected from the tapetum increases (Fig. 3c, evaluated at $\lambda = 555$ nm) and the reflected color redshifts (Fig. 3d, e). The color shift from $\lambda_{acidic, avg} = 482 \pm 8$ nm to $\lambda_{basic, avg} = 556 \pm 6$ nm is induced by an increase in the lattice constant of the photonic lattice due to progressively increased electrostatic repulsion[2]. On the contrary, within acidic/basic regimes, both the intensity and the

reflected wavelength are less affected by the gradual pH changes thus resulting in a mostly invariant optical response of the tapetum (Fig. 3b–e). In acidic conditions the intensity of the reflected light evaluated at $\lambda = 555$ nm is lower than in basic conditions possibly due to the compression of a portion of the lattice that induces a shift of the reflected light to the UV range and thus decreases the amount of reflected light in the visible range. Due to the natural variability of the tapetum, the entity of the color shift slightly changes from sample to sample and within the same tissue due to local variations of the photonic structure (e.g., lattice parameters, orientation). For extremely basic conditions (pH > 10), there is a slight decrease in the intensity of the reflected light; this phenomenon is attributed to the onset of the degradation of the collagen fibrils which causes the photonic crystal to degrade as well and, therefore, induces a decrease in the reflectance intensity[47].

The color of the tapetum can also be reversibly modulated across the visible range. The pH swing between acidic and basic conditions was obtained by alternatively immersing the tapetum in 0.025 M HCl (pH ~ 1.9) and 0.1 M NaOH (pH ~ 12) (Fig. 3f). Consistently with what was observed for the pH gradient, an acidic environment causes the tapetum to reflect light more blue-
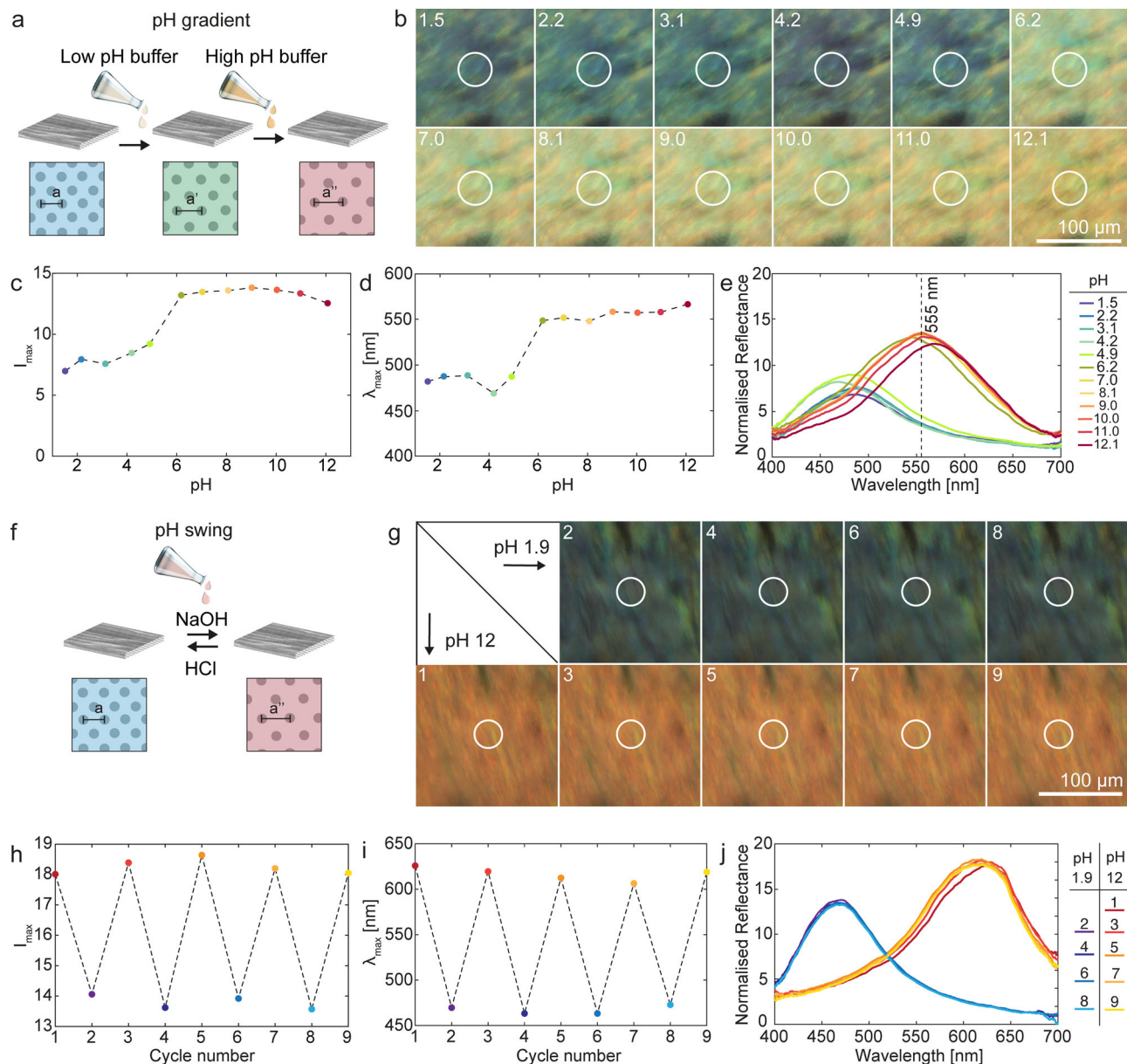
Fig. 3 Chemical control of spectral response in soft photonic systems. a Schematic representation of the pH gradient driven structural changes in the tapetum's photonic lattice obtained by immersing the tapetum in citric acid and disodium phosphate buffer progressively adjusted with sodium hydroxide and hydrochloric acid to span the pH range 1.5–12.1. **b** Optical micrographs of the tapetum observed in bright field reflection after immersion in the buffer. White circles correspond to the spectral collection spot (diameter 45 μm). **c** Maximum intensity (I_{max}) and **d** corresponding wavelength (λ_{max}) as a function of each investigated pH value evaluated at $\lambda = 555$ nm showing a bimodal distribution of values. **e** Normalized reflectance as a function of wavelength for each investigated pH value. **f** Schematic representation of the pH swing driven structural changes in the tapetum's photonic lattice obtained by alternatively immersing the tapetum in sodium hydroxide and hydrochloric acid. **g** Optical micrographs of the tapetum observed in bright field reflection after immersion in base (pH 12) and acid (pH 1.9) for nine cycles. White circles correspond to the spectral collection spot (diameter 33 μm). **h** Maximum intensity (I_{max}) and **i** corresponding wavelength (λ_{max}) as a function of the cycle number. **j** Normalized reflectance as a function of wavelength for each cycle.

shifted compared to the light reflected by the tapetum in a basic environment due to the tighter packing of the collagen fibrils (Fig. 3g–j). The tapetum reversibly switched coloration between blue and red with $\lambda_{acidic,\ avg} = 467 \pm 5$ nm and $\lambda_{basic,\ avg} = 616 \pm 7$ nm for up to nine times (Fig. 3i, j) with consistently higher reflectance intensity in basic than in acidic conditions (Fig. 3h).

Electric field driven dynamic behavior of soft photonic systems. Electronics are the gold-standard interface for the control of displays. Their use is adapted as an interface to these naturally occurring spectrally responsive systems. Electrode arrays are directly placed on the surface of the tapetum to locally generate electric fields for local and reversible control of the tapetum's spectral response (Fig. 4, Supplementary Fig. S9). For applied voltages >1.23 V, water hydrolysis occurs; this is expected to induce a pH gradient perpendicular to the electrodes that grows over time[48]. In particular, a basic environment should form in the proximity of the anode while an acidic environment in the proximity of the cathode. Thus, different regions of the tapetum should experience different pH values, depending on their distance from the electrodes[16]. This electrically generated pH gradient is expected to affect the photonic lattice of the tapetum
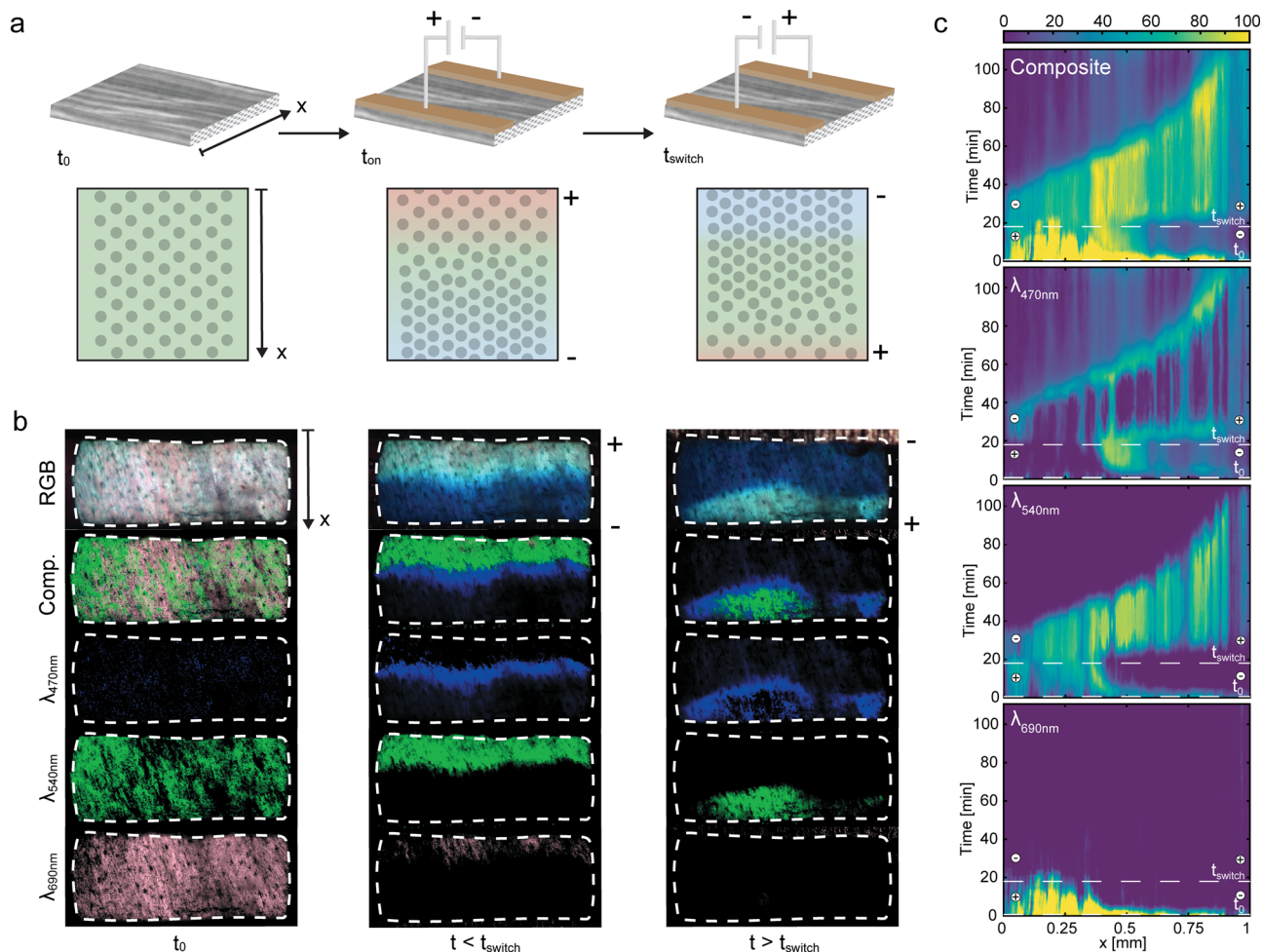
Fig. 4 Electrical control of spectral response in soft photonic systems. a Schematic representation of the electrical stimulation of bovine tapetum (top row) and corresponding representation of the tapetum cross-section (bottom row) as a function of time and electrodes' polarity. When no voltage difference is applied (t_0) the tapetum optical appearance is homogeneous with respect to the electrodes; upon application of a voltage difference of 3 V acidification occurs at the cathode ($t < t_{switch}$) inducing a blue-shift of the reflected color in the proximity of the cathode; upon electrodes polarity switching the acidification region is reversed ($t > t_{switch}$). **b** RGB and false-color (Composite, $\lambda = 470$, 540, and 690 nm) bright-field reflection micrographs of the region of tapetum circle between the electrodes at $t = t_0$, $t < t_{switch}$, and $t > t_{switch}$. **c** Time-resolved grayscale intensity as a function of horizontal position for the middle line profile (Supplementary Fig. S12) of the tapetum for the composite map, $\lambda = 470$ nm, $\lambda = 540$ nm, and $\lambda = 690$ nm. Color bar corresponds to a grayscale intensity between 0–100.

consistently with what was previously observed by immersing the tapetum in pH buffers and in acidic/basic solutions. This implies that in correspondence of the acidic environment of the cathode the tapetum is more tightly packed and displays a blue reflectance, while in the proximity of the basic environment of the anode the tapetum is less tightly packed and its coloration is more red-shifted. To demonstrate this hypothesis a bovine tapetum circle (diameter 5 mm) was interfaced with Au-electrode arrays with a channel length $l = 1$ mm (Supplementary Fig. S9); the response of the tapetum in the region between the electrodes was monitored as a function of time t in three conditions: (i) with no applied voltage difference between the electrodes, (ii) with 3 V voltage difference applied at time $t = t_{on}$, and (iii) with the same voltage difference but switching the electrodes' polarity at $t = t_{switch}$ (Fig. 4a). Three main reflective components were identified in the tapetum before the application of the voltage difference: blue ($\lambda_{blue, max} = 470$ nm), green ($\lambda_{green, max} = 540$ nm), and pink ($\lambda_{pink, max} = 690$ nm) (Supplementary Fig. S10). Multispectral analysis of the individual spectral components was performed for the three regimes (Fig. 4b, c and Supplementary Figs S11, S12, and Supplementary Movie 1). This analysis offers a detailed

visualization method of the spectral response distribution in the tapetum as a function of time and space (Fig. 4c) by plotting the intensity of the grayscale value for each image corresponding to a specific spectral component as a function of time.

For $t < t_{on}$, the texture of the tapetum is striated and with no heterogeneity induced by the presence of the gold electrodes, as demonstrated also by multispectral analysis of the tapetum circle (Fig. 4b, left). Also, under no applied electric field, the main reflectance of the tapetum is centered between 540-690 nm, with minimal reflection in the blue portion of the visible range (Fig. 4b, left, Fig. 4c). Upon application of the electric field, for $t_{on} < t < t_{switch}$, the optical appearance of the tapetum is asymmetric perpendicularly to the electrodes with a redshifted region in proximity of the anode and a blue-reflecting region in proximity of the cathode (Fig. 4b, middle). This is exemplified by the multispectral analysis which shows an asymmetric distribution of color with strong green and pink signals in the proximity of the anode and blue signal further away from it (Fig. 4c). Upon switching of the polarity of the electrodes, for $t > t_{switch}$, the acidic and basic regions are reversed, thus reversing the color gradient on the tapetum and inducing a redshift of the reflected color with

respect to the spectral response at $t_{on} < t < t_{switch}$ (Fig. 4b, right). Interestingly, the reflectance contribution in the pink spectral region is minimal, thus implying the lattice is more compressed compared to $t < t_{switch}$ (Fig. 4c).

Conclusion

This work reports the study of the spectral response and the dynamic control of soft, curvilinear photonic systems based on the *Bos taurus* tapetum ex vivo with both chemical and electrical strategies. The spectral variations induced are reversible and affect the entire surface area of the tapetum when exposed to a specific pH environment, while patterned responses can be obtained using electrode arrays. The evolution of the color change in variable pH environments and electric fields is visualized using multispectral imaging. The ability to reversibly tune flexible photonic crystal adds insight for the development of soft, curvilinear photonic materials that exhibit dynamic spectral response and radiative energy management while elucidating fundamental processes that occur in living systems such as the animals' actual vision ability and their capacity to adapt to environments with varying and/or extreme illumination conditions. These structures provide examples that can be used as inspiration for the fabrication of membranes with controlled optical response, with utility in soft bioinspired displays, camouflage, and electronic skins.

Methods

Materials. Citric acid, sodium phosphate, sodium hydroxide and hydrochloric acid were purchased from Sigma-Aldrich (USA) and used as received without further purification. Deionized water with a resistivity of 18.2 MΩ cm^{-1} and pH of 6.6 was obtained with a Milli-Q reagent-grade water system and used to prepare aqueous solutions.

Animal handling. Commercially available fixed bovine *Bos taurus* eyes taken from cattle slaughtered for beef production (U.S. origin, <24 months old) were acquired from Carolina®. The tapeta were isolated from the ocular bulbs by dissection following a standard protocol for mammals' eyes: briefly, first the vitreous humor, the lens, and the retina were removed; then the tapetum and the choroid were peeled off from the sclera. The tapeta were left attached to the choroid for easier manipulation. Free-standing tapeta were rinsed with Carolina Perfect Solution® (pH 7) and stored in the same solution at room temperature until further use. Before any experiment the eyes were rinsed abundantly with Milli-Q water (pH 6.6) and kept hydrated with water or with a dedicated solvent during optical analysis as specified for each experiment. To demonstrate the relative spatial arrangement of the tapetum and of the retina, a portion of the retina was left on the tapetum for the scanning electron microscopy analysis reported in the image of Supplementary Fig. S2.

Macroscopic photographs. Digital macroscopic images of the bovine tapeta were taken with a smartphone (iPhone 5, Apple) and adjusted for exposure and contrast.

Optical microscopy and spectroscopy. A customized Olympus inverted IX71 microscope equipped with a digital single-lens reflex (DSLR) camera (Canon Rebel EOS-SL1) and with a halogen lamp (Olympus, U-LH100L-3) as light source was used to perform optical microscopy. Bright-field reflection images were collected using 10× (Olympus, UPlanFL N, NA = 0.3), 20× (Olympus, LUCPlanFL N, NA = 0.45), and 50× (Olympus LMPlanFL N, NA = 0.5) objectives. To quantify the reflectance of the bovine tapeta, the microscope was coupled to a spectrometer (Ocean optics, USB2000) through an optical fiber (Ocean Optics, P600-2-UV-VIS, 600 μm core size, conjugated spot diameter for the 20x objective is 33–45 μm) mounted in confocal configuration. The reflectance spectra were normalized against a silver mirror (PF10-03-P01-10, Thorlabs) immersed in Milli-Q water. The spectra were smoothed and plotted using the software MATLAB R2021a.

To perform multispectral analysis of the static optical response reported in Fig. 2 and Supplementary Fig. S3, an Olympus IX71 microscope was coupled to a multispectral camera (CRI Nuance EX). The tapeta were observed using a 40× objective (Olympus, LUCPlanFL N, NA = 0.6) in bright field reflection and the spectral maps were acquired in the range 450–750 nm with a step size of 5 nm. The software Nuance 3.0.2 was used to acquire and unmix the maps in different spectral components and the software MATLAB R2021a and ImageJ were used to analyze the data. The spectra were normalized with respect to each curve's maximum.

To perform multispectral analysis of the static optical response reported in Fig. 4, Supplementary Figs. S10–S12, an Olympus SZ STU-2 stereo microscope coupled to a multispectral camera (CRI Nuance EX) was used in brightfield

reflection at 3× magnification. The spectral maps were acquired in the range 450–750 nm with a step size of 10 nm.

FTIR. Bovine tapeta were characterized by Fourier Transformed Infrared Spectroscopy (FTIR) recorded by a Bruker ALPHA II FTIR spectrometer, with an attenuated total reflectance unit (Platinum-ATR unit) after rinsing in Milli-Q water and drying. For each measurement, 64 scans were coadded with a resolution of 4 cm^{-1}, in the interval 400−4000 cm^{-1}. Only the spectral information in the interval 900−1800 cm^{-1} was reported to better visualize the amide peaks.

Prism coupling. A Metricon waveguide instrument (2010/M) was used to evaluate the average index of refraction of the dry and wet bovine tapeta. The measured index of refraction was evaluated at a wavelength of $\lambda = 632.8$ nm generated by a HeNe laser and using a 930.7* prism ($n_{TE} = n_{TM} = 1.965$). The bovine tapeta were rinsed with Milli-Q water and either measured while still wet ($n_{tapetum, wet}$) or dried overnight before the measurement ($n_{tapetum, dry}$).

Scanning electron microscopy. Bovine tapeta were rinsed with Milli-Q water, dried, and blade-cut to expose a fresh cross-section. The fragments were mounted on aluminum stubs using carbon tape to be at 90° with respect to the electron beam. To ensure electrical conductivity, the stubs were sputtered with ~8–10 nm of gold using an Emitech SC7620 sputter coater. The top view and the cross-sections of the dried tapeta were imaged using a Zeiss EVO MA10 Scanning Electron Microscope (SEM) with a secondary electron detector at 10 kV with 6–7.5 mm as the working distance.

Transmission electron microscopy. Bovine tapeta for plastic-embedded sectioning and transmission electron microscopy (TEM) were obtained from excised tapeta using 3 mm surgical punches and kept in Carolina perfect solution. Tapetal samples were then post-fixed in 2% osmium tetroxide for 15 min, dehydrated in acetone, and then infused with Spurr resin. Thin sections (70–100 nm) were captured on copper grids and stained with 4% uranyl acetate and then Reynolds lead citrate. Thin sections were imaged on a JEOL 100CX transmission electron microscope with a Gatan ORIUS camera.

pH control. For the pH gradient and the pH swing, 5 mm diameter tapeta discs were cut from excised tapeta using surgical punches. The discs were then put in 3.5 cm polystyrene Petri dishes and covered with solutions. Each solution was added in excess, to completely cover the tapeta. The reflectance spectra were collected imaging through the Petri dish and from the central part of the tapeta punches to avoid damaged (e.g., compressed or frayed) regions at the edges.

For the pH gradient curve, 0.1 M citric acid and 0.2 M Na$_2$HPO$_4$ buffers (citrate-phosphate buffer) were dropwise adjusted with 10 M NaOH (pH > 8) and 1 M HCl (pH < 3) to prepare solutions at pH 1.5, 2.2, 3.1, 4.2, 4.9, 6.2, 7.0, 8.1, 9.0, 10.0, 11.0, and 12.01. The pH value of each prepared solution was measured using a pH meter probe (Seven Multi, Mettler Toledo). The tapetum samples were left to equilibrate for 5 min in each buffer solution before acquiring the spectral response; after that, the solvent at each pH was completely removed before the addition of the next pH solution. The calibration curve (Fig. 3C) was built evaluating the tapetum reflectance intensity spectrum for each pH datapoint at $\lambda = 555$ nm and extrapolating the corresponding reflectance intensity (I_{max}).

For the pH swing, 0.025 M HCl (pH = 1.9) and 0.1 M NaOH (pH = 12.1) solutions were used to induce the transition from basic to acidic conditions. The 5 mm diameter tapetum samples were left to equilibrate for 10 min in each buffer solution before acquiring the spectral response; after that, the solvent at each pH was completely removed before the addition of the next pH solution.

Electrical stimulation. For the electrical stimulation 5 mm diameter punched tapeta hydrated with Milli-Q water were placed in direct contact (colored side facing the gold) with gold electrode arrays (channel electrode width $w = 1.8$ mm, spacing $l = 1$ mm) connected to a power supply through alligator clips. The electrode arrays were prepared by depositing Cr/Au ($t_{Au} = 100$ nm with a chromium adhesion layer with thickness $t_{Cr} = 10$ nm) on glass slides (15-550-A3, 25 × 75 × 1mm, Fisherbrand), covered with a vinyl mask (Oracal), prepared using the Silhouette Cameo precision cutter. The glass slides were plasma etched (Zepto, Diener Electronic) to clean the substrate and ensure better adhesion before the deposition of the metallic layers. The voltage difference between the electrodes was generated by using a source meter (Keithley 26535 A) with an applied DC voltage of 3 V. The voltage value was chosen to be higher than the water electrolysis potential (1.23 V, 25 °C) and, at the same time, low enough to minimize the formation of bubbles for imaging purposes. The tapeta were observed for up to 110 min and the electrodes' polarity was switched after 18 min (t_{switch}). Multispectral maps were acquired in the spectral range 450–750 nm, with a step size of 10 nm, and a 40 s interval between each map giving in total 167 multispectral maps.

Image processing. The software ImageJ was used to obtain the grayscale intensity as a function of space of the multispectral maps acquired for the electrical stimulation of the tapetum. Briefly, each of the 167 multispectral maps was unmixed in a blue ($\lambda_{blue, max} = 470$ nm), green ($\lambda_{green, max} = 540$ nm), and pink ($\lambda_{pink,}$

$_{max}$ = 690 nm) false-color image. Each image was imported in ImageJ and a stack was created for each spectral component. The function "line profile" was used to extrapolate the grayscale value (0–255 range) as a function of space for each image of the stack. The software MATLAB R2021a was then used to smooth and plot the profiles as image matrices.

Data availability

All data sets are available in the main text, in the supplementary materials, or from the corresponding author upon reasonable request.

References

1. Kinoshita, S. *Structural Colors in the Realm of Nature. Structural Colors in the Realm of Nature* (World Scientific, 2008).
2. Kinoshita, S., Yoshioka, S. & Miyazaki, J. Physics of structural colors. *Reports Prog. Phys.* **71**, 076401 (2008).
3. Joannopoulos, J. D., Johnson, S. G., Winn, J. N. & Meade, R. D. *Photonic Crystals: Molding the Flow of Light. Photonic Crystals: Molding the Flow of Light* 2nd edn (Princeton University Press, 2011).
4. Teyssier, J., Saenko, S. V., Van Der Marel, D. & Milinkovitch, M. C. Photonic crystals cause active colour change in chameleons. *Nat. Commun.* **6**, 6368 (2015).
5. Gur, D. et al. Light-induced color change in the sapphirinid copepods: tunable photonic crystals. *Adv. Funct. Mater.* **26**, 1393–1399 (2016).
6. Gur, D. et al. The mechanism of color change in the Neon Tetra fish: a light-induced tunable photonic crystal array. *Angew. Chemie Int. Ed.* **54**, 12426–12430 (2015).
7. Stokkan, K. A. et al. Shifting mirrors: adaptive changes in retinal reflections to winter darkness in Arctic reindeer. *Proc. R. Soc. B Biol. Sci.* **280**, 20132451–20132451 (2013).
8. Lopez-Garcia, M. et al. Light-induced dynamic structural color by intracellular 3D photonic crystals in brown algae. *Sci. Adv.* **4**, eaan8917 (2018).
9. Vigneron, J. P. et al. Switchable reflector in the Panamanian tortoise beetle Charidotella egregia (Chrysomelidae: Cassidinae). *Phys. Rev. E Stat. Nonlin. Soft Matter Phys.* **76**, 031907 (2007).
10. Mäthger, L. M., Collins, T. F. T. & Lima, P. A. The role of muscarinic receptors and intracellular Ca2+ in the spectral reflectivity changes of squid iridophores. *J. Exp. Biol.* **207**, 1759–1769 (2004).
11. Mathger, L. M. Rapid colour changes in multilayer reflecting stripes in the paradise whiptail, Pentapodus paradiseus. *J. Exp. Biol.* **206**, 3607–3613 (2003).
12. McDougal, A., Miller, B., Singh, M. & Kolle, M. Biological growth and synthetic fabrication of structurally colored materials. *J. Optics (United Kingdom)* **21**, 073001 (2019).
13. Berthier, S. *Iridescences: The Physical Colors of Insects* (Springer New York, 2007).
14. Rassart, M., Simonis, P., Bay, A., Deparis, O. & Vigneron, J. P. Scale coloration change following water absorption in the beetle Hoplia coerulea (Coleoptera). *Phys. Rev. E Stat. Nonlin. Soft Matter Phys.* **80**, 031910 (2009).
15. Tamáska, I. et al. Color changes upon cooling of lepidoptera scales containing photonic nanoarchitectures, and a method for identifying the changes. *J. Insect Sci.* **13**, 87 (2013).
16. Nucara, L., Greco, F. & Mattoli, V. Electrically responsive photonic crystals: a review. *J. Mater. Chem. C* **3**, 8449–8467 (2015).
17. Isapour, G. & Lattuada, M. Bioinspired stimuli-responsive color-changing systems. *Advanced Materials* **30**, 1707069 (2018).
18. Hanlon, R. T. & Messenger, J. B. *Cephalopod Behaviour* (Cambridge University Press, 2018).
19. Cuthill, I. C. et al. The biology of color. *Science* **357**, eaan0221 (2017).
20. Pedler, C. The fine structure of the tapetum cellulosum. *Exp. Eye Res.* **2**, 189–IN46 (1963).
21. Land, M. F. & Nilsson, D.-E. Animal eyes. *Exp. Clin. Psychopharmacol.* **1**, 173–187 (1993).
22. Ollivier, F. J. et al. Comparative morphology of the tapetum lucidum (among selected species). *Veterinary Ophthalmology* **7**, 11–22 (2004).
23. Lesiuk, T. P. & Braekevelt, C. R. Fine structure of the canine tapetum lucidum. *J. Anat.* **136**, 157–164 (1983).
24. Yamaue, Y., Hosaka, Y. Z. & Uehara, M. Macroscopic and histological variations in the cellular tapetum in dogs. *J. Vet. Med. Sci.* **76**, 1099–1103 (2014).
25. Schwab, I. R., Yuen, C. K., Buyukmihci, N. C., Blankenship, T. N. & Fitzgerald, P. G. Evolution of the tapetum. *Trans. Am. Ophthalmol. Soc.* **100**, 187–99 (2002). discussion 199-200.
26. Bernstein, E. H., Pease, L. C. & Bernstein, M. H. Electron microscopy of the Tapetum Lucidum of the cat. *J. Cell Biol.* **5**, 35–39 (2004).
27. Coles, J. A. Some reflective properties of the tapetum lucidum of the cat's eye. *J. Physiol.* **212**, 393–409 (1971).
28. Braekevelt, C. R. Fine structure of the Bovine Tapetum fibrosum. *Anat. Histol. Embryol.* **15**, 215–222 (1986).
29. Hogg, C. et al. The eyes of the deep diving hooded seal (Cystophora cristata) enhance sensitivity to ultraviolet light. *Biol. Open* **4**, 812–818 (2015).
30. Benson, K. & Suter, R. B. Reflections on the tapetum lucidum and eyeshine in lycosoid spiders. *J. Arachnol.* **41**, 43–52 (2013).
31. Land, M. F. A multilayer interference reflector in the eye of the scallop, Pecten maximus. *J. Exp. Biol.* **45**, 433–447 (1966).
32. Oron, D. et al. The image-forming mirror in the eye of the scallop. *Science* **358**, 1172–1175 (2017).
33. Somiya, H. Fishes with eye shine: functional morphology of Guanine type tapetum Lucidum. *Mar. Ecol. Prog. Ser.* **2**, 9–26 (2007).
34. Gur, D. et al. The dual functional reflecting Iris of the Zebrafish. *Adv. Sci.* **5**, 1800338 (2018).
35. Locket, N. A. The choroidal tapetum lucidum of Latimeria chalumnae. *Proc. R. Soc. London Biol. Sci.* **186**, 281–290 (1974).
36. Braekevelt, C. R. Fine structure of the choriocapillaris, Bruch's membrane and retinal epithelium of the cow. *Anat. Histol. Embryol.* **15**, 205–214 (1986).
37. Carolina. *Carolina Mammal Eye Dissection Guide* (Carolina, 2005).
38. Guidetti, G., Sun, H., Marelli, B. & Omenetto, F. G. Photonic paper: multiscale assembly of reflective cellulose sheets in Lunaria annua. *Sci. Adv.* **6**, eaba8966 (2020).
39. Guidetti, G. et al. Unmixing octopus camouflage by multispectral mapping of Octopus bimaculoides' chromatic elements. *Nanophotonics* **10**, 2441–2450 (2021).
40. Johansen, V. E. et al. Genetic manipulation of structural color in bacterial colonies. *Proc. Natl. Acad. Sci. USA* **115**, 2652–2657 (2018).
41. Schertel, L. et al. Complex photonic response reveals three-dimensional self-organization of structural coloured bacterial colonies. *J. R. Soc. Interface* **17**, 20200196 (2020).
42. Bosak, A., Snigireva, I., Napolskii, K. S. & Snigirev, A. High-resolution transmission X-ray microscopy: A new tool for mesoscopic materials. *Adv. Mater.* **22**, 3256–3259 (2010).
43. Fratzl, P. in *Collagen: Structure and Mechanics* (ed. Fratzl, P.) 1–13 (Springer, Boston, MA, 2008).
44. Wang, X. Group refractive index measurement of dry and hydrated type I collagen films using optical low-coherence reflectometry. *J. Biomed. Opt.* **1**, 212 (1996).
45. Etherington, D. J. & Sims, T. J. Detection and estimation of collagen. *J. Sci. Food Agric.* **32**, 539–546 (1981).
46. Bellairs, R., Harkness, M. L. R. & Harkness, R. D. The structure of the tapetum of the eye of the sheep. *Cell Tissue Res.* **157**, 73–91 (1975).
47. Bowes, J. H. & Kenten, R. H. The swelling of collagen in alkaline solutions; swelling in solutions of univalent bases. *Biochem. J.* **46**, 524–529 (1950).
48. Forster, R. J. & Keyes, T. E. *Handbook of Electrochemistry* (Elsevier, 2007).

Author contributions

Conceptualization: F.G.O., G.G. Methodology: G.G., C.P., G.M., G.E.B., B.J.M., B.N., F.G.O. Investigation: G.G., C.P., G.M., G.E.B., B.J.M., B.N. Visualization: G.G., F.G.O. Funding acquisition: F.G.O. Project administration: F.G.O. Supervision: G.G., F.G.O. Writing—original draft: G.G., F.G.O. Writing—review and editing: G.G., F.G.O.

Competing interests

The authors declare no competing interests.

Additional information

Supplementary information The online version contains supplementary material available at https://doi.org/10.1038/s43246-022-00305-8.

Correspondence and requests for materials should be addressed to Fiorenzo G. Omenetto.

Peer review information *Communications Materials* thanks Mikhail Inyushin and the other, anonymous, reviewer(s) for their contribution to the peer review of this work. Primary Handling Editor: Aldo Isidori.

Reprints and permission information is available at http://www.nature.com/reprints